The Accuracy of Marine Shadow-Band Sun Photometer Measurements of Aerosol Optical Thickness and Ångström Exponent

MARK A. MILLER, MARY JANE BARTHOLOMEW, AND R. MICHAEL REYNOLDS

Brookhaven National Laboratory, Upton, New York

(Manuscript received 21 May 2003, in final form 8 September 2003)

ABSTRACT

An analytical uncertainty propagation model is used in conjunction with laboratory and field data to quantify the uncertainty in measurements of the direct-normal irradiance, aerosol optical thickness, and Ångström exponent made with a ship-mounted fast-rotating shadow-band radiometer (FRSR). Total uncertainties in FRSR measurements of aerosol optical thickness are found to be 0.02–0.03 at the 95% confidence level (two standard deviations). The ''lever-arm'' effect, a salient characteristic of the Langely technique in which uncertainties in aerosol optical thickness measurements are reduced as the solar zenith angle increases, is essentially offset by orientation uncertainty. Lack of a lever-arm effect precludes Langley calibration of FRSRs while at sea; they must be calibrated on land. Uncertainties in FRSR measurements of the two-wavelength Ångström exponent are shown to depend strongly on the aerosol optical thickness, with the maximum uncertainty of 0.6 associated with clean, maritime air masses.

1. Introduction

Measurements of the transmissivity of aerosols in the visible and near-infrared wavelengths over the world's oceans are needed to evaluate satellite estimates of aerosol radiation transfer properties used in climate and ocean color studies (King et al. 1999; Gordon and Wang 1994). Over-water measurements are difficult and, until recently, only a few usable measurements existed. The number of over-ocean measurements of aerosol optical properties is expanding due to the development and implementation of new shipboard instruments: handheld sun photometers (Porter et al. 2001; Deschamps et al. 2002) and marine fast-rotating shadow-band radiometers (FRSRs; Reynolds et al. 2001). Handheld sun photometers are collimated instruments that are pointed at the solar disk by an operator and measure the direct beam irradiance. In contrast, FRSRs and other shadow-band radiometers measure the direct-beam irradiance by decomposing the irradiance field into its direct and diffuse components (Guzzi et al. 1985; Harrison et al. 1994). Unlike handheld sun photometers, FRSRs are designed for long-term, unattended deployments. There are currently 5–10 FRSRs deployed on various ships across the world's oceans at any given time.

Radiometry on a ship has the special problem of platform motion. A large research vessel typically will have a periodic rocking motion with a period of 5–10 s and a standard deviation of $\pm 1°$–$5°$ about a mean tilt angle of $\pm 1°$–$2°$, which is related to weight distribution, wind forcing, and the directional wave field. The motion stability will change slowly over hours or days, and more suddenly when the ship changes direction abruptly. Handheld sun photometers operated on ships rely on the human operator for orientation and stabilization, while the FRSR relies on careful monitoring of ship motion and compensation for it in the radiation measurements. There are several different methods of monitoring platform motion ranging from a gyroscope to fluid-based pitch and roll sensors. Cost and operating environment are important issues when selecting the motion monitoring apparatus. In addition to platform motion, the optical detector system used on an operational device like the FRSR is subject to the harsh environmental conditions encountered on the ship's deck. This can cause drift in the detector circuitry, diffuser optical properties, or interference filters. Finally, the ship's effluent can cause problems through deposition on the diffuser or contamination of the atmospheric signal.

This paper addresses uncertainty in marine FRSR measurements of aerosol optical thickness, $\tau_{\lambda A}$. Subjects ranging from the impact of platform motion on measurement uncertainty through uncertainties in calibration are discussed. A lofty goal, on land as well as at sea, is to measure $\tau_{\lambda A}$ with an uncertainty of approximately 0.02 for solar zenith angles from 0° to 70° ($3 \geq m \geq 1$, where m is the atmospheric air mass; $m \cong \sec\theta_e$). The basic issues that generate uncertainty are examined using an analytical uncertainty propagation model. This

Corresponding author address: M. A. Miller, Brookhaven National Laboratory, Bldg. 490d, Upton, NY 11973.
E-mail: miller@bnl.gov

analysis provides a framework for interpretation of marine FRSR measurements by the atmospheric and oceanographic sciences communities.

2. Marine FRSR uncertainty analysis

The reduction in the intensity of solar radiation as it passes through the atmosphere is quantified by the optical thickness, τ_λ, where λ is the wavelength. Using Beer's solution to Lambert's extinction law, $I_{\lambda N} = I_{\lambda T} \exp(-m\tau_\lambda)$, yields

$$\tau_\lambda = m^{-1}[\ln(I_{\lambda T}) - \ln(I_{\lambda N})], \tag{1}$$

where $\tau_\lambda = \tau_{\lambda A} + \tau_{\lambda R} + \tau_{\lambda O} + \tau_{\lambda C}$. In this expression, the subscripts *A*, *R*, *O*, and *C* indicate the contributions to the optical thickness made by aerosols, molecular scattering (Rayleigh), ozone absorption, and clouds, respectively. The variable *m* is referred to as the air mass and is approximately equal to $\sec\theta_e$ for solar zenith angles less than 70°, where θ_e is the solar zenith angle relative to the earth's coordinate system. Here, $I_{\lambda N}$ is the measured irradiance of the solar beam referenced to a plane that is normal to the solar beam (excluding all scattered diffuse light), and $I_{\lambda T}$ is the top-of-the-atmosphere irradiance prior to interaction with atmosphere. With the exception of *m* (under typical conditions), each term in (1) is wavelength dependent, as indicated by the subscript λ. A coefficient known as the Ångström exponent, α, describes the wavelength dependence of $\tau_{\lambda A}$. The Ångström exponent (Ångström 1961) can be computed in many ways and in this paper is defined as

$$\alpha = \frac{\ln(\tau_2/\tau_1)}{\ln(\lambda_1/\lambda_2)}, \tag{2}$$

where the subscripts 1 and 2 refer to two different wavelengths, λ_1 and λ_2.

Much about marine FRSR uncertainty can be learned from a simple theoretical model based on uncertainty propagation (Meyer 1992, chapter 10). The standard deviation, σ_x, is used in this paper to represent any uncertainty in the measurement, systematic or random, of *x*. The variance equation for $z = f(x, y)$ about point *P* is

$$\sigma_z^2 \approx \left(\frac{df}{dx}\right)_P^2 \sigma_x^2 + \left(\frac{df}{dy}\right)_P^2 \sigma_y^2, \tag{3}$$

where *x* and *y* are independent variables and all covariances are assumed to be 0. This is the formula employed in this paper to propagate uncertainty. In this paper, the terms in (3) are computed using the maximum values as determined analytically or from measurements, thereby yielding a ''worst case'' estimate of the uncertainty in the standard deviation of the measured quantity. If a covariance existed in the variance equation, it would contribute in a manner that would compound this worse-case estimate, but this scenario is unlikely in the problem at hand.

The first step is to derive the variance equations for τ_λ and α for a sun photometer. The irradiance at the top of the atmosphere can be written as $I_{\lambda T} = I_{\lambda 0}(r_0/r)^2$, where $I_{\lambda 0}$ is the mean irradiance for the mean earth–sun distance, r_0. The variable *r* is the earth–sun distance at the time of the measurement. Substituting this into (1) and solving for $\tau_{\lambda A}$ yields

$$\tau_{\lambda A} = \frac{1}{m}\left[\ln I_{\lambda 0} - \ln I_{\lambda N} - 2\ln\left(\frac{r_0}{r}\right)\right] - \tau_{\lambda R} - \tau_{\lambda O} - \tau_{\lambda C}. \tag{4}$$

When the Langley method (Shaw 1983; Harrison and Michalsky 1994; Schmidt and Wehrli 1995) is used, the optical thicknesses are assumed constant during a sunrise and sunset, and a plot of $\ln(I_{\lambda N})$ versus *m* can be extrapolated to $m = 0$ so as to provide an estimate of $\ln(I_{\lambda T})$. It is possible to cast (4) in terms of voltage rather than irradiance, thereby eliminating the radiometer calibration as a source of uncertainty, although a case can be made for using irradiance for the purpose of gathering data that can be used to test radiative transfer codes for atmospheres containing aerosol, one of the applications of the FRSR. A second advantage of using irradiance rather than voltage is that the absolute calibration of the radiometer can be compared to previously measured values of top-of-the-atmosphere irradiance.

According to (3), the variance of (4) is

$$\sigma_{\tau_{\lambda A}}^2 = \left(\frac{1}{m}\right)^2\left[\left(\frac{\sigma_{I_{\lambda 0}}}{I_{\lambda 0}}\right)^2 + \left(\frac{\sigma_{I_{\lambda N}}}{I_{\lambda N}}\right)^2\right] + \sigma_{\tau_{\lambda R}}^2 + \sigma_{\tau_{\lambda O}}^2 + \sigma_{\tau_{\lambda C}}^2, \tag{5}$$

which is nearly identical to Eq. (11) in Russell et al. (1979) and similar in structure to Eq. (A15a) derived in Russell et al. (1993), although the variables propagated are different in the latter. It is assumed that $\sigma_m^2 \simeq 0$ since the geographic position of the radiometer and the time of the observation are known to a high degree of accuracy. Also, astronomical distances are well known and do not fluctuate on the same scale as $\sigma_{\tau_{\lambda A}}^2$, so $\sigma^2 r_0/r \simeq 0$. As discussed in the appendix, failure to correct for $\tau_{\lambda R}$ and $\tau_{\lambda O}$ in certain wavelength bands will severely impact the absolute value of $\tau_{\lambda A}$, but $\tau_{\lambda R}$ and $\tau_{\lambda O}$ are known to reasonable accuracy and fluctuate slowly, so their contribution to measurement *uncertainty* in a collection of measurements from a single day is negligible (i.e., $\sigma_{\tau_{\lambda R}}^2 \simeq \sigma_{\tau_{\lambda O}}^2 \simeq 0$). Efforts are made to measure $\tau_{\lambda A}$ in cloud-free conditions, so $\sigma_{\tau_{\lambda C}}^2 = 0$.

The corresponding variance equation for α from (2) is

$$\sigma_\alpha^2 = \left[\ln\left(\frac{\lambda_1}{\lambda_2}\right)\right]^{-2}\left[\left(\frac{\sigma_{\tau_{\lambda_1}}}{\tau_{\lambda_1}}\right)^2 + \left(\frac{\sigma_{\tau_{\lambda_2}}}{\tau_{\lambda_2}}\right)^2\right]. \tag{6}$$

Equations (5) and (6) are used to evaluate the uncertainty in marine FRSR measurements. Because σ_α^2 is a

function of $\sigma^2_{\tau_{\lambda A}}$, the task is reduced to determining $\sigma^2_{\tau_{\lambda A}}$, or more fundamentally $\sigma^2_{I_{\lambda 0}}$ and $\sigma^2_{I_{\lambda N}}$. In the sections that follow, the magnitudes of $\sigma^2_{I_{\lambda N}}$ and $\sigma^2_{I_{\lambda 0}}$ are examined; the foundation for these estimates is the transfer equation of a marine FRSR, which is discussed in the following section.

a. The transfer equation of a marine shadow-band radiometer

The marine FRSR described in this paper incorporates a seven-channel (one broadband, six 10-nm narrowband) silicon-detector-based optical head and a semicircular occulting arm. The occulting arm circumscribes a complete rotation centered on the optical head, thereby occulting a band of the sky, with a revisitation period of 6.5 s. The signals from all seven optical channels are sampled rapidly so the shadow cast by the shadow band onto the detectors can be recognized and recorded. Reynolds et al. (2001) describe the marine FRSR and develop all of the mathematics required to compute τ_λ. Two irradiance measurements must be determined from the high-speed-sampled data stream during the shadow-band sweep over the upper hemisphere. These are the edge irradiance, $I_{\lambda E}$, and the shadow irradiance, $I_{\lambda S}$. The ''edge'' irradiance is defined as the most representative value of the measured irradiance when the shadow band is adjacent to, but not occulting, the solar disk. Platform tilt measurements in the form of pitch and roll are recorded twice each shadow-band revolution. Finally, mean values of the platform's latitude, longitude, and heading are measured.

The direct-normal irradiance for an FRSR is

$$I_{N,\lambda} = \frac{I_{\lambda E} - I_{\lambda S}}{\chi(\phi_r, \theta_r)\cos\theta_r}, \tag{7}$$

where the function $\chi(\phi_r, \theta_r)$ is a cosine correction factor for the optical head and ϕ_r and θ_r are the solar azimuth and zenith relative to the instrument, respectively (Fig. 1). The diffuser material may have non-Lambertian scattering properties that combine with filter and detector geometry to slightly alter the cosine response of the instrument; these effects are quantified by $\chi(\phi_r, \theta_r)$. The cosine correction term is provided by the manufacturer as a ϕ_r, θ_r lookup table unique to each detector in the head. An important feature in the design of the marine shadow-band radiometer is that $I_{\lambda E}$ and $I_{\lambda S}$ compensate for the diffuse irradiance blocked by the shadow band and are measured in a few tenths of a second, so there is a negligible change in the ϕ_r, θ_r pair during the measurement. This compensation for the diffuse irradiance is not perfect if the diffuse field is highly anisotropic, which occasionally occurs when the atmosphere is highly polluted or the solar zenith angle is large. It is acceptable under most circumstances, though.

A linear calibration equation is used to convert from electronic analog-to-digital converter output to measured irradiance, that is, $I_\lambda = g_\lambda v_\lambda + b_\lambda$, where v_λ is the analog-to-digital converter output, g_λ is the calibration gain, and b_λ is the offset. The calibration equation is derived from factory calibrations of the optical head and from electronic calibrations, and the resulting calibration is unique to each of the seven channels in the head. For a given FRSR, the electronic calibration changes by only a few tenths of a percent over a year of operation while changes in the calibration of the optical head are considerable and systematic, providing one of the major sources of uncertainty. The optical head calibration issues will be discussed later. From this point on, the subscript λ refers to one of the six narrowband channels, and the wavelength-dependent irradiance, I_λ, refers to the mean irradiance weighted by the wavelength response of the channel, given by

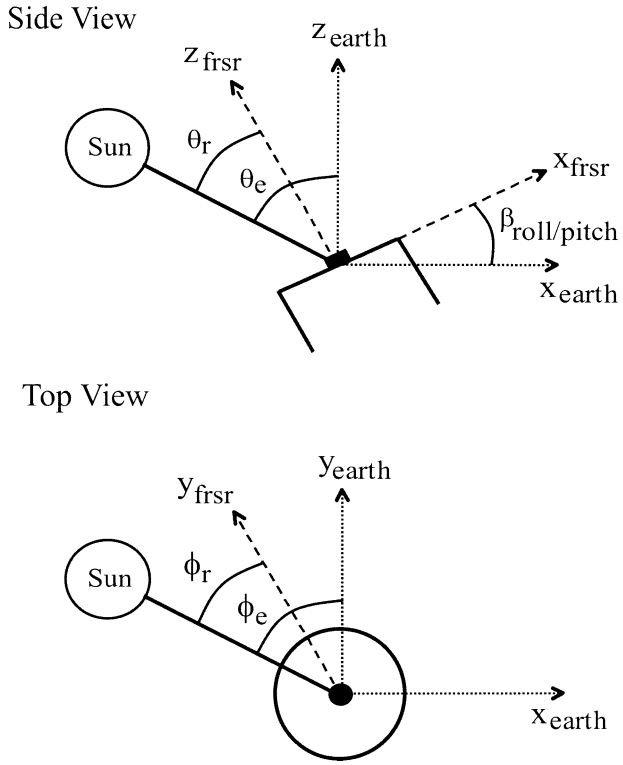

FIG. 1. The geometry of a shadow-band radiometer operated on a moving platform.

$$I_\lambda = \frac{\int I(\lambda)w(\lambda)\,d\lambda}{\int w(\lambda)\,d\lambda}. \tag{8}$$

The passband response $w(\lambda)$ is provided by the manufacturer and integration is made over the passband range.

Following (7), the actual direct-normal beam irradiance is

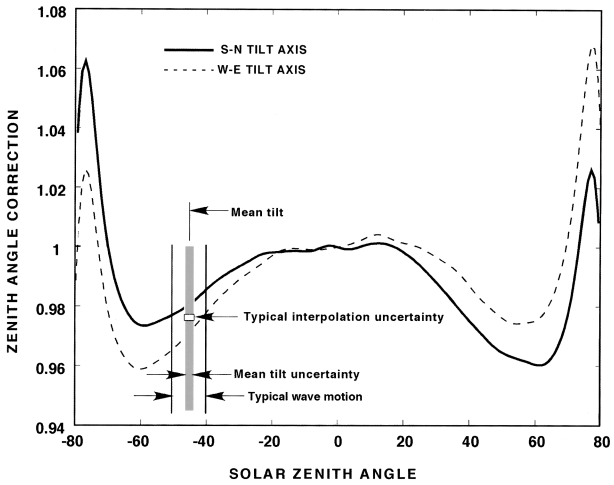

FIG. 2. Typical angle correction, $\chi(\theta_r, \phi_r)$, for an FRSR. The correction is measured using a light beam and rotating the head over 180°, through south-to-north and east-to-west planes, in 1° steps. Differences between the two planes come from nonsymmetry in the location of the silicone cells with respect to the foreoptic diffuser. Contamination of the diffuser will affect the correction terms. Shown are envelopes of the typical wave motion and mean tilt uncertainty, which are derived from 2-min averages of the raw platform motion data. Also indicated are the mean tilt and the uncertainty in the mean tilt.

$$I_{N,\lambda} \simeq \frac{g_\lambda \Delta v_\lambda}{\chi(\theta_r)\cos\theta_r}, \tag{9}$$

where $\Delta v_\lambda = v_{\lambda E} - v_{\lambda S}$; its functional dependencies are discussed later. While the functional dependence of χ on ϕ_r appears to be similar in magnitude to its dependence on θ_r (Fig. 2), the ship's angular motion would have to be tens of degrees to realize this dependence. Since the ship's angular excusions are only a few degrees, the functional dependence of χ on ϕ_r is small and will be henceforth neglected. Additional evidence provided later in the paper shows that even if the functional dependence were to be of the same magnitude as the functional dependence on θ_r, compared to other factors it would still be a negligible factor in the total uncertainty in the measurement of $\tau_{\lambda A}$.

The procedure for computing θ_r and ϕ_r begins with a calculation of solar azimuth, ϕ_e, and solar zenith angle, θ_e, in the earth's coordinate system from the latitude, longitude, and time. These angles are used to compute the Cartesian coordinates of a solar beam vector of unit length in the earth's coordinate system. The well-documented rotational coordinate transformation matrix, $\mathbf{T}$, for three independent rotations, maps the radiometer-following coordinate system to the earth's coordinate system. The components of the solar beam vector in the earth's coordinate system are converted to the platform frame of reference by inverting $\mathbf{T}$. The outputs of this conversion are the x_r, y_r, and z_r components of a unit vector representing the position of the sun relative to the radiometer normal. The radiometer-relative solar zenith angle is computed using $\theta_r = \arccos(z_r)$.

The transfer equation given by (9) describes a marine FRSR in which the position of the radiometer is precisely monitored as the band occults the sun during each sweep. This equation represents the best possible equipment configuration, but not the most cost effective. The marine FRSR was designed to be a robust, reasonably priced, autonomous instrument that could be integral to a global ship observing network. Instantaneous measurements of pitch, roll, and heading require sophisticated instrumentation, beyond the design goals, to separate true rotation from linear accelerations common in wave motion. A compromise is to use a damped-fluid, pitch–roll sensor and average all pitch and roll measurements over a 2-min time period. Pitch and roll of the ship in a wave field is random, while mean tilt is systematic. The 2-min averaging time is sufficient to reduce the 5–10-s wave-induced motions to an acceptable level, leaving the much slower mean tilts that result from ship list and wind–wave pressures. Averaging over 2 min eliminates the random element, leaving the mean tilt as a residual. As shown in Reynolds et al. (2001), this averaging provides an acceptable motion correction. Each pitch–roll sensor is calibrated at the factory. Temperature dependency is less than 0.5° over a 10°–50° range. FRSRs are installed on large research vessels on which mean tilts are usually less than 2° and rocking seldom exceeds 5°. In these conditions, the 2-min-averaged pitch and roll have a combined systematic and random uncertainty of approximately 0.5°.

The instantaneous direct-beam irradiance onto a horizontal surface is estimated by

$$\langle I_{\lambda,H}\rangle \approx \langle I_{\lambda,E}\rangle - \langle I_{\lambda,S}\rangle = g_\lambda \langle \Delta v_\lambda\rangle, \tag{10}$$

where the angle brackets indicate an average over the 2-min interval. Following (7), the resulting equation for computing the normal-beam irradiance becomes

$$\langle I_{N,\lambda}\rangle \simeq \frac{g_\lambda \langle \Delta v_\lambda\rangle}{\chi_r(\phi_r, \theta_r)\langle\cos\theta_r\rangle}. \tag{11}$$

The implications of averaging on the uncertainty will be discussed in later sections. The variance of $\langle I_{\lambda N}\rangle$ is

$$\sigma^2_{\langle I_{N,\lambda}\rangle} \simeq \left(\frac{g_\lambda\langle\Delta v_\lambda\rangle}{\chi\langle\cos\theta_r\rangle}\right)^2 \left[\underbrace{\left(\frac{\sigma_{g_\lambda}}{g_\lambda}\right)^2}_{\text{gain}} + \underbrace{\left(\frac{\sigma_{\langle\Delta v_\lambda\rangle}}{\langle\Delta v_\lambda\rangle}\right)^2}_{\text{edge shadow}} + \underbrace{\left(\frac{\sigma_{\langle\cos\theta_r\rangle}}{\langle\cos\theta_r\rangle}\right)^2}_{\text{orientation}}\right]. \tag{12}$$

In this expression, the cosine correction term $(\sigma_{\chi_r}/\chi_r)^2$ has been omitted because it is negligible compared to the other terms within the operating range of the FRSR ($\theta_e < 65°$). In fact, one reason that the operating range is limited to $\theta_e < 65°$ is to avoid the strongly nonlinear portion of the cosine correction term. Omission of the cosine correction term can be justified by examining the magnitude of actual cosine correction terms $\chi_r(\phi_r, \theta_r)$,

for a typical FRSR (Fig. 2). Figure 2 shows an exaggerated range for typical wave motion (~10°) over a 2-min averaging period. Observations that fall within this 2-min period are averaged to produce an estimate of the mean tilt, as shown. This mean tilt is subject to 0.5° measurement uncertainty that occurs because the cosine correction term, χ_r, must be interpolated between laboratory measurements. This figure shows that $\sigma_{\chi_r} \approx 0.005$ and $\chi_r \simeq 0.98$, so $(\sigma_{\chi_r}/\chi_r)^2 \simeq 2.6 \times 10^{-5}$ in the calculation of $\sigma^2_{\langle I_{N,\lambda}\rangle}$. In contrast, the other terms in brackets are shown later to be of the order of 10^{-4}, an order of magnitude larger than $(\sigma_{\chi_r}/\chi_r)^2$, thereby justifying its omission. These magnitudes have been confirmed using a model of χ_r formed by summing multiple Gaussian functions, using it to compute $(\sigma_{\chi_r}/\chi_r)^2$, and including $(\sigma_{\chi_r}/\chi_r)^2$ in (12). Results show that the uncertainty in the cosine correction term is not a signficant contributor to measurement under typical conditions. Recent comparisons have shown, however, that the cosine correction function itself does change significantly over time, perhaps due to changes in the optical properties of the diffuser material, and research to determine the magnitude of these changes and their impact on uncertainty in $\langle I_{N,\lambda}\rangle$ is ongoing.

b. Gain uncertainty

The terms g_λ and $\sigma^2_{g,\lambda}$ in (12) are the actual value and uncertainty of the wavelength-dependent optical and electronic gain, g_λ. The gain uncertainty is a function of many factors, including the optical properties of the Spectralon diffuser and interference filters, which can change with time when exposed to the elements. Compared to the changes in these optical properties, the gain drift due to the electronic circuitry behind the detectors is negligible. The detector of the FRSR is calibrated using a National Institute of Standards and Technology (NIST) bulb. These bulbs have a reported absolute accuracy of 0.6%, although more conservative estimates are made in the literature (Schmidt and Wehrli 1995). The manufacturer of the FRSR head quotes the gain uncertainty to be 2%, which is reinforced by FRSR comparison experiments performed as part of calibration exercises related to various FRSR deployments.

Experience has shown that the gain of some FRSR heads may drift by a considerable amount (>10%) during long deployments (several months), so it is imperative that the heads be frequently calibrated. Techniques have been developed to track the drift in the FRSR head gain by comparing the data from the FRSR's broadband channel with a more stable broadband instrument. While this technique is sensitive to drift in the λ response of the diffuser and interference filters and to water vapor contributions in broadband measurements, it can be used qualitatively to access whether the observed gain drift was gradual or instantaneous over the period of deployment. If the amount of the drift in the head gain is known from pre- and postcruise calibrations, it can be accounted for so as to reduce gain uncertainty. The procedure used is to apply a linear correction factor bounded at the beginning and the end of the cruise by the calibrations. The appropriateness of this linear interpolation can be judged qualitatively by examining the broadband comparisons. Although calculations are performed for higher gain uncertainties, the typical gain uncertainty is assumed to be 2%. A 2% gain uncertainty most often represents a freshly calibrated FRSR during its first few weeks of deployment.

c. Edge-shadow voltage uncertainty

The edge-shadow uncertainty term quantifies uncertainty associated with making the measurement of the edge-shadow voltage difference. Because the FRSR must employ a band to occult the sun, some of the diffuse irradiance is inadvertently occulted. Therefore, an actual measurement of the diffuse field cannot be made, although, as discussed previously, the edge-shadow technique is used to estimate the amount of band-occulted diffuse irradiance allowing the diffuse field to be estimated. The procedure that is currently used for this estimate is to record the time series of the voltage for each individual 6.5° sweep of the occulting band through the sun during a 2-min averaging period (Fig. 3a). Away from the sun, the band is occulting the global irradiance field, but as it sweeps across the solar disk it occults the direct-beam irradiance (the shadow), along with a small part of the diffuse irradiance field. The voltage time series for a series of individual sweeps during the 2-min averaging period can result in simple, well-defined edge and shadow voltages (Fig. 3a) or more complicated configurations (Figs. 3b,c). Some of the physical factors that cause variations in the edge-shadow time series from one sweep to the next are revealed by combining (4) and (9). The resulting expression is

$$\widetilde{\Delta v}_\lambda = I_{\lambda 0}\chi g_\lambda^{-1}(r_0/r)^2 \times \cos\theta_r \exp[-(\tau_{\lambda A} + \tau_{\lambda R} + \tau_{\lambda O} + \tau_{\lambda C})\sec\theta_e], \quad (13)$$

where $\widetilde{\Delta v}_\lambda$ is the instantaneous voltage difference. This expression shows that instantaneous edge-shadow voltage $\widetilde{\Delta v}_\lambda$ should be impacted by platform motion through its dependence on θ_r. The other variables in (13) vary slowly and do not change from one sweep to the next. Hence, it is anticipated that a series of individual sweeps will differ from one another due to platform motion; if there is no motion, the individual sweeps should be almost identical to one another.

Strictly speaking, expression (13) does not provide a complete picture of the mechanisms that must be considered when operating an actual FRSR. The edge-shadow concept is relatively simple to implement when the scattering characteristics of the aerosol do not vary from the edge of the solar disk on one side of the sun to the

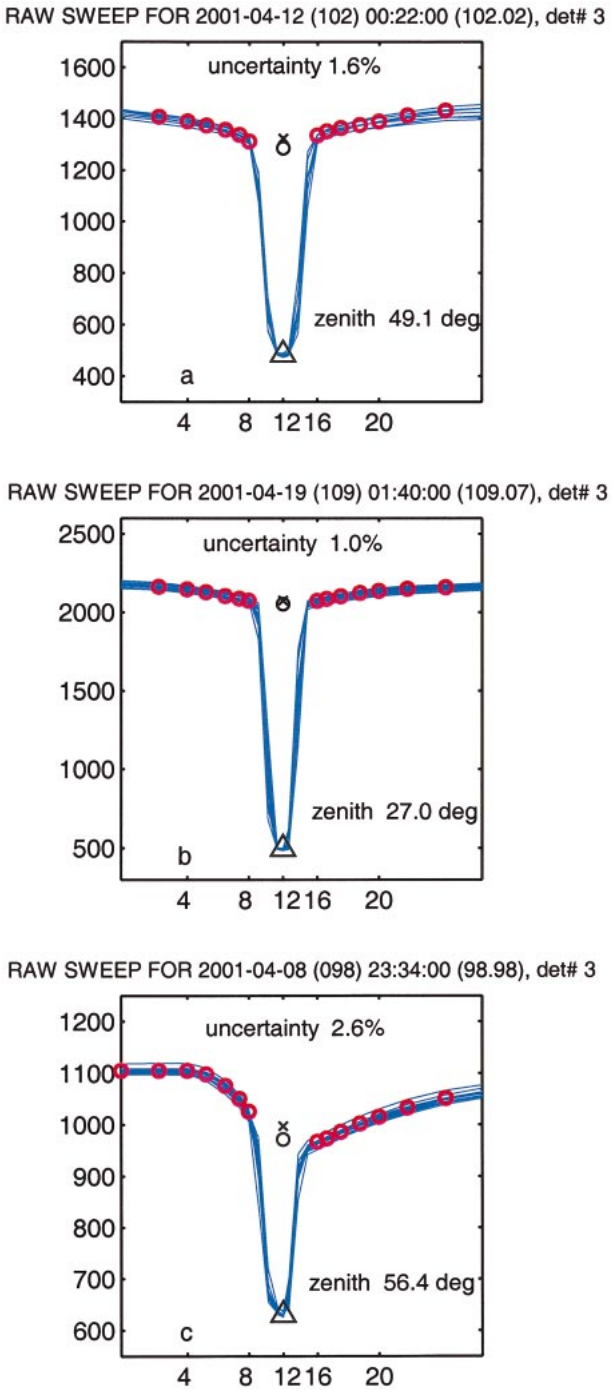

FIG. 3. (a)–(c) Several raw voltage time series that were used in a 2-min average. Not all of the 18 sweeps during the 2-min averaging pass initial filtering. The bold circles indicate the best voltage estimate for each time index and the circle at index 12 is the edge voltage using a spline fit of the average voltages (bold circles) along the two edges. The x marks the position of a simple linear interpolation, which was used in early versions of the FRSR processing software. The triangle marks the average value of the shadow voltage. The uncertainty is computed using the sum of the standard deviations of the two edge values observed just before and after the shadow and the standard deviation of the shadow voltage. This sum of standard deviations is divided by the edge-shadow voltage determined using the spline fit and converted to a percentage.

edge of the solar disk on the other. It becomes more complicated if the aerosol has a pronounced directional phase function (Fig. 3c) or if the sun is low in the sky. In the latter case, if the ship's motion geometry is such that the band sweeps from top to bottom across the solar disk, there will be a large gradient in the geometric pathlength traversed by photons originating just above the upper and just below the lower edge of the solar disk. In these cases, the edge voltage may be quite different from one side of the sun to the other. In practice, we employ a spline interpolation across the shadow region to produce the best estimate.

Inspection of the voltage time series plots when the solar zenith angle is low (sun is high in the sky) and there is little rocking (Fig. 3a) shows that there is little variation in the shadow voltages. This is expected because the shadow voltage is composed of diffuse irradiance only, although a small portion of the diffuse irradiance is occulted by the imperfect shape of the band. The integrated diffuse irradiance is not directional. Conversely, there is considerable sweep-to-sweep variability in the edge voltages in the time series (Fig. 3a) due to platform motion as suggested by (13). The motion impacts the direct-beam irradiance, which is the major contributor to the edge voltage.

The edge-shadow voltage uncertainty, $(\sigma_{\langle \Delta v_\lambda \rangle}/\langle \Delta v_\lambda \rangle)^2$, quantifies how well the correct edge and shadow voltages can be estimated from the time series data collected during the 2-min averaging period. If the sweep time series is simple and has little sweep-to-sweep variability, the selection of the edge and shadow values is straightforward and there is little uncertainty ($<1\%$). This usually occurs when there is little rocking, the solar zenith angle is low, and optical thickness values are less than 0.2. If the FRSR is stationary (on land), the uncertainty is due exclusively to natural variability in the atmospheric properties and uncertainties are 0.5% or less. The sweep-to-sweep variability in the edge voltage increases when the ship is subject to increased rocking (Fig. 3c). Individual sweeps are averaged to eliminate the impact of instantaneous wave motion, thereby producing an average voltage time series consistent with the mean tilt angle of the ship during the 2-min averaging period. The standard deviation of the edge voltage time series essentially represents the uncertainty in the edge-shadow voltage measurement because the standard deviation of the shadow voltage is so much smaller. Typical values of this uncertainty when the ship is rocking normally are ~1%–2% in most circumstances.

The time series shape may become even more complex due to strong scattering by aerosols in close proximity to the direct-beam vector, which may occur when the optical thickness is large (>0.5). In this case, the directional scattering phase function of the aerosols creates a large halo around the sun and may cause the edge voltages from one side of the sun to the other to be asymmetrical (Fig. 3c). Under these circumstances, the selection of the edge voltage can become rather com-

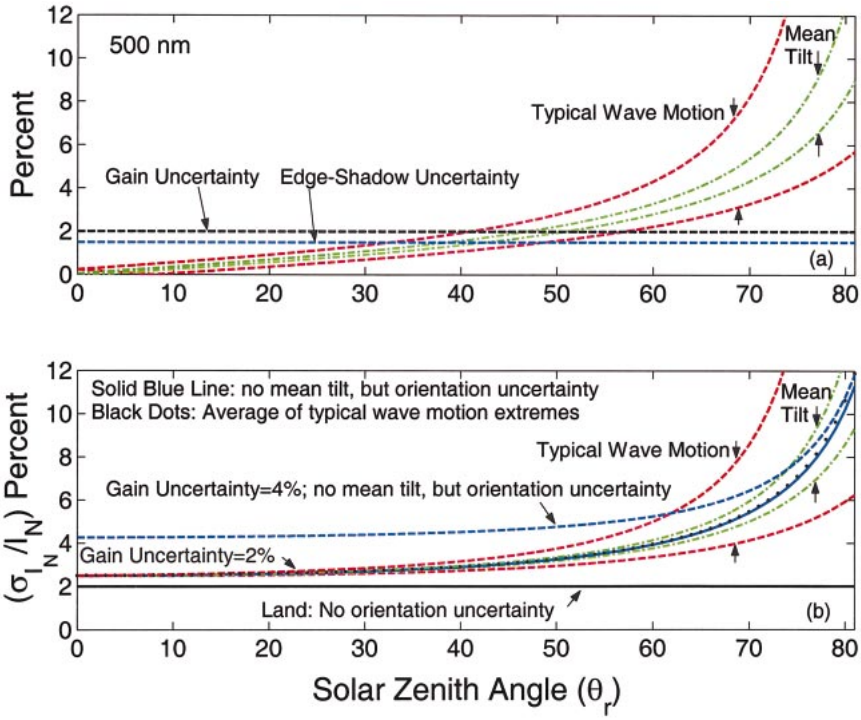

FIG. 4. (a) The individual components of uncertainty in the FRSR measurement of the direct-normal irradiance, $I_{\lambda N}$, as a function of the solar zenith angle, θ_e. The uncertainty in instrument gain (black dashed line) is 2%, and the uncertainty in the edge-shadow voltage measurement is 1.5% (blue dashed line). The orientation uncertainty envelopes for typical wave motion (red dashed lines, roll or pitch angles of $\pm 8°$) and typical mean tilt (green dashed lines, roll or pitch angles of $\pm 2°$) are plotted. (b) As in (a) but for the combined effects of gain, edge-shadow, and orientation uncertainty. The black dots result from averaging the typical wave motion ($\pm 8°$), which is a random variable; this exercise demonstrates that averaging these random waves essentially causes no bias due to the cosine response of the radiometer. The blue dashed line represents a doubling of the gain uncertainty to 4% (edge-shadow voltage uncertainty remains 1.5%). The solid black line shows the result when there is no orientation uncertainty (land), while the gain uncertainty and edge-shadow uncertainty are 2% and 1.5%, respectively.

plicated, introducing additional uncetainty, occasionally as much as 3%. The spline fit produces a better estimate of the edge voltage (Fig. 3c) and improves performance in cases when the optical thickness is unusually large. This improved performance has been documented in extensive comparisons with handheld columnated sun photometers in highly polluted conditions.

In summary, the edge-shadow voltage uncertainty is determined by several factors, including the rocking motion of the ship, the performance of the software that determines the edge-shadow voltages, the solar zenith angle, and the optical thickness. We can estimate uncertainty from the data; in clear conditions it is ~1%–2%, but in exceptional cases it can be as much as 3%.

d. Orientation uncertainty

Uncertainties in the exact specification of θ_r are due to uncertainties in the measurements of heading (β_h), pitch (β_p), and roll (β_r) angles. It is possible to estimate the impact of these uncertainties using

$$\sigma^2_{\cos\theta_r} \simeq \{\cos[\theta_r(\beta_r + \Delta\beta_r, \beta_p)] - \cos[\theta_r(\beta_r - \Delta\beta_r, \beta_p)]\}^2, \quad (14)$$

where $\Delta\beta_r$ is the accuracy specification of the roll transducers as supplied by the manufacturer and θ_r is computed using the procedure outlined above. The roll is used in (14) because it is typically larger than the pitch, but the angle used in this calculation is arbitrary; motion along either axis has the same effect on the uncertainties. The orientation uncertainty is minimized at low solar zenith angles due to the shape of the cosine function, as shown in the next section.

UNCERTAINTY IN THE DIRECT-NORMAL IRRADIANCE, $(\sigma_{I_{\lambda N}}/I_{\lambda N})^2$

The percentage uncertainty in the direct-normal irradiance can be computed using (12) and (14), a gain uncertainty of 2%, and an edge-shadow voltage uncertainty of 1.5%. A range of calculations were performed for different wave conditions (Fig. 4). The orientation

term was computed for θ_rs of 0°, ±4°, and ±8°, which represent the full range of wave motion typically observed on ship carrying FRSRs. Orientation uncertainty (Fig. 4a) occupies an envelope bounded by the −8° and 8° angles; note that the minimum at 8° represents a situation when the roll angle is exactly the solar zenith angle, so the uncertainty in the radiometer's position straddles the radiometer normal and (14) is 0. This envelope represents the orientation uncertainty for typical instantaneous wave motions. As noted, these individual wave motions are averaged over a 2-min period so as to determine the mean tilt, which is normally ±2°. The envelope of the orientation uncertainty for the mean tilt is considerably more narrow (Fig. 4a).

When the solar zenith angle is between 40° and 55°, the orientation uncertainty surpasses the gain uncertainty and, thereafter, dominates the uncertainty in the direct-normal irradiance measurement (Fig. 4a). The 2% gain uncertainty is not a function of the solar zenith angle and produces a 3% uncertainty in $I_{\lambda N}$ that is compounded at high zenith angle by the orientation uncertainty (Fig. 4b). It is possible to derive a good estimate of the impact of averaging the typical wave motions to determine the mean tilt by averaging the uncertainty estimates for the ±8° extremes (black line with black dots). Comparing this calculation with that representing no wave motion, but orientation uncertainty (solid blue line), shows that the averaging procedure nearly approximates the uncertainty in $I_{\lambda N}$ in the ''no motion'' scenario (0° roll), as discussed in Reynolds et al. (2001). This suggests that averaging the typical wave motions over a 2-min period, assuming they are random, does not produce a significant averaging bias due to the cosine response of the radiometer. Degradation in the gain uncertainty to 4% from 2% (dashed blue line) essentially doubles the percent uncertainty in the $I_{\lambda N}$ measurement at solar zenith angles less than 30° showing that gain drifts occurring during long deployments may significantly impact instrument accuracy.

In summary, averaging and using the mean tilt for the platform correction apparently results in a minor increase in the uncertainty of the direct-normal irradiance. Future FRSRs should be capable of instantaneous corrections for each sweep. Note that the 2%–3% uncertainty in $(\sigma_{\langle I_{N,\lambda}\rangle}/\langle I_{N,\lambda}\rangle)^2$ due to the gain uncertainty alone (Fig. 4a, black line) is presumably the uncertainty in this measurement if the FRSR were mounted on land.

3. Uncertainty in the aerosol optical thickness and Ångstrom exponents

To compute the uncertainty of the aerosol optical thickness, $\sigma^2_{\tau_{\lambda A}}$, it is necessary to specify the value of the direct-normal irradiance, $I_{\lambda N}$, which can be obtained from (4) as

$$\langle I_{\lambda N}\rangle = I_{\lambda 0}\left(\frac{r_0}{r}\right)^2 \exp[-m(\tau_{\lambda A} + \tau_{\lambda R} + \tau_{\lambda O})], \quad (15)$$

where clear-sky conditions are assumed ($\tau_C = 0$). The value of $I_{\lambda N}$ is dependent on the season [i.e., through $(r_0/r)^2$] and the aerosol optical thickness, $\tau_{\lambda A}$. It also depends on the Ångström exponent, α, which describes the wavelength dependence of $\tau_{\lambda A}$. The values of $I_{\lambda 0}$ used here and in calculations performed below are taken from Thullier et al. (2003, hereafter THU). Although the seasonality correction factor is negligibly small, the date is assumed to be 21 December 2000 for the simulations shown in the rest of this paper. Neglecting molecular scattering and ozone components in accordance with the appendix, (5) is written as

$$\sigma^2_{\tau_{\lambda A}} = \left(\frac{1}{m}\right)^2\left[\left(\frac{\sigma_{I_{\lambda 0}}}{I_{\lambda 0}}\right)^2 + \left(\frac{\sigma_{\langle I_{\lambda N}\rangle}}{\langle I_{\lambda N}\rangle}\right)^2\right], \quad (16)$$

which is used hereafter.

a. Uncertainty in the extraterrestrial irradiance, $(\sigma_{I_{\lambda 0}}/I_{\lambda 0})^2$

An important application of the FRSR is to provide evaluation data for radiative transfer codes. These codes assume an extraterrestrial irradiance spectrum at the top of the atmosphere and allow this incoming radiation stream to interact with atmospheric aerosols (or cloud particles) for the purpose of determining the vertical profile of heating in the atmosphere and the quantity of radiation that eventually reaches the surface. There are a number of published extraterrestrial spectra, sometimes based on satellite radiation measurements. Therefore, it is imperative that the irradiance measurements made by the FRSR be constrained by the same extraterrestrial irradiance spectrum used in radiation transfer models, or by a close approximation with known biases relative to widely used spectra.

A problem arises when the best published values for the extraterrestial spectral solar irradiance differ by a significant amount (Fig. 5). Most of the disagreement in the published spectra occur in the blue-yellow (<600 nm) and in the near-infrared (>800 nm) regions. The data in Table 1 where obtained by convolving the spectral response functions for the bands in a typical FRSR head with the published solar spectra. The variability in the estimates in Table 1 reflects a combination of instrument uncertainty and variation in the solar output spectrum. The $I_{\lambda 0}$ values for 415 nm have a difference of 4.6% over the range shown—for 500 nm, 2.3%; for 615 nm, 2.6%; for 670 nm, 1.9%; and for 870 nm, 7.3%. The measurements of the extraterrestial solar spectrum made from space (Colina et al. 1996; Thuillier et al. 1998; THU) are considered to be the best. From these, the THU values are chosen as the reference spectrum for the FRSR because the data were collected during four different missions, thereby making this the largest and most comprehensive dataset to date.

As previously mentioned, $I_{\lambda 0}$ for sun photometers is generally determined through the Langley technique. As discussed below, however, the Langley technique cannot be used to calibrate FRSRs at sea due to orientation

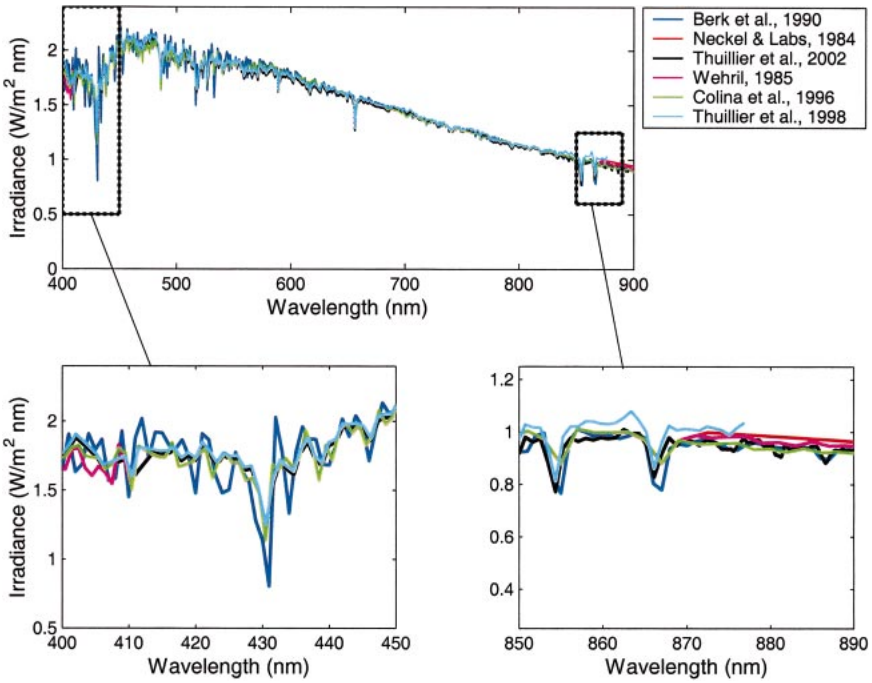

FIG. 5. A comparison of six different extraterrestrial solar spectral irradiances (W m^{-2}) as a function of wavelength. The two lower illustrations are high-resolution plots of the 400–450- (violet-blue) and 850–890-nm (near-infrared) regions of the spectrum.

uncertainty. Langley plots for the FRSR must be performed on land. Langley calibrations of FRSRs on land at Mauna Loa, Hawaii; Mount Lemmon, Arizona; and on the roof of building 490D at the Brookhaven National Laboratory, Upton, New York, generally provide values of $I_{\lambda 0}$ that agree within 1%–2% of the THU values. Accordingly, the $I_{\lambda 0}$s used to process FRSR data are derived by convolving the instrument bandpass with the THU values, rather than through frequent Langely analyses, as would be the case on land. The instrument gain change is estimated using pre- and postcruise calibrations and adjusted in the data in postprocessing, in an attempt to maintain a calibration consistent with the THU values. At sea, aerosol optical thickness measurements are also compared with handheld sun photometer data (when it is available) to track drift, and FRSRs are calibrated in a laboratory as frequently as possible. For the purpose of linking FRSR irradiances to radiation codes, it is appropriate to assume on the basis of experience and the values in Table 1 that the uncertainty in the absolute extraterrestrial calibration for a typical FRSR is approximately 1.5%, assuming that the THU values are accurate. Because there is significant uncertainty in the solar reference spectra itself, this uncertainty could be significantly larger, particularly at 870 nm, whereupon later calculations show results for uncertainites of 1.5% and 3.0% for guidance.

TABLE 1. The different estimates of $I_{\lambda 0}$ from the literature. Six different solar spectra are presented here. Each spectrum was convolved with the bandpass transfer function from a typical 10-nm filter. The mean irradiance (W m^{-2}) for the six estimates and the percent difference from the means are shown for each radiometer band. The current "best" estimate of $I_{\lambda 0}$ is THU, which is significantly different than other spectra for important wavelengths.

λ (nm)	Mean	NL84	W85	B90	C96	T98	T03
415	1.75	−1.03	−1.14	3.31	−0.80	1.14	−1.25
500	1.95	−0.51	−0.67	−0.20	−0.46	1.04	0.26
615	1.70	0.76	0.65	−0.06	0.76	−0.47	−1.82
670	1.53	0.20	0.07	0.59	0.20	0.20	−1.31
870	0.96	0.52	0.10	−2.91	−1.04	4.16	−1.04
940	0.83	5.21	−2.42	−0.36	−0.24	−2.42	−0.12

NL84, Neckel and Labs (1984).
W85, Wehril (1985).
B90, Berk et al. (1990).
C96, Colina et al. (1996).
T98, Thuiller et al. (1998).
T03, THU.

b. Results

Calculations of $\sigma_{\tau_{\lambda A}}$ for several different situations were performed (Fig. 6). The first experiment shows $\sigma_{\tau_{\lambda A}}$ for optimal FRSR operating conditions, when the uncertainty in the extraterrestrial irradiance is 1.5% and the gain uncertainty is 2%. Calculations for 0°, ±2°, and ±8° were made, representing the envelopes of typical wave motion, mean tilt, and no motion. The envelope of $\sigma_{\tau_{\lambda A}}$ is quite narrow through solar zenith angles of 60°, but degrades rapidly at low solar zenith angles in the ±8° case (typical wave motion). Conversely, 2°

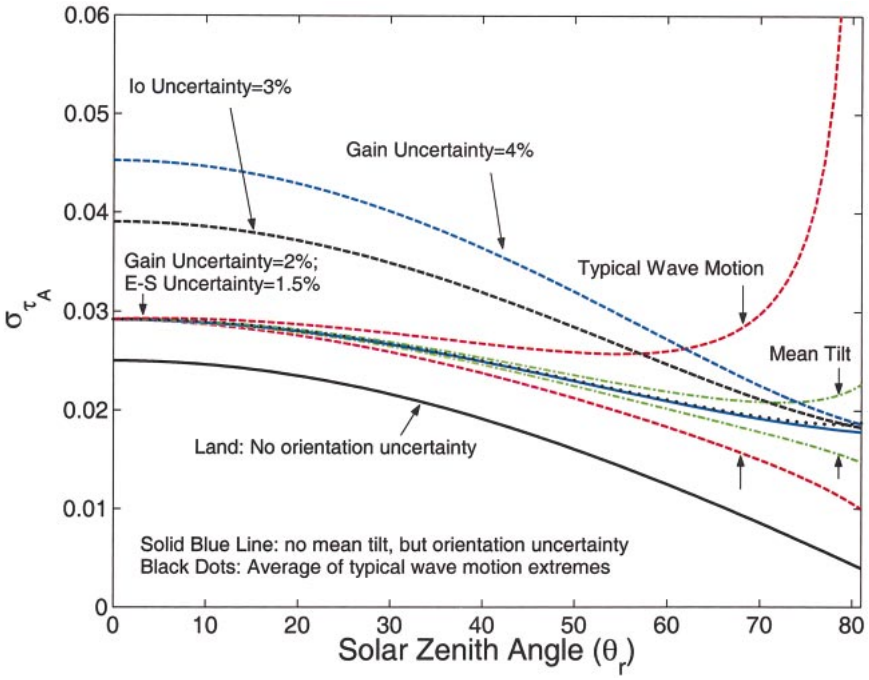

FIG. 6. The uncertainty in the FRSR measurement of aerosol optical thickness, $\tau_{\lambda A}$, as a function of solar zenith angle, θ_e. Under typical circumstances, the uncertainty in instrument gain is 2%, the uncertainty in the edge-shadow voltage measurement is 1.5%, and the uncertainty in the extraterrestrial irradiance is 1.5% (family of curves indicated in plot). The orientation uncertainty envelopes for typical wave motion (red dashed lines, roll or pitch angles of $\pm 8°$) and typical mean tilt (green dashed lines, roll or pitch angles of $\pm 2°$) are plotted. The black dots result from averaging the typical wave motion ($\pm 8°$), which is a random variable; this exercise demonstrates that averaging these random waves essentially causes no bias due to the cosine response of the radiometer. The blue dashed line represents a doubling of the gain uncertainty to 4% (edge-shadow voltage uncertainty remains 1.5%). The black dashed line represents a doubling of the uncertainty in the extraterrestrial irradiance to 3%.

uncertainty in the mean tilt produces a negligible effect on $\sigma_{\tau_{\lambda A}}$ as compared to the no-motion case. Averaging the $\pm 8°$ typical wave motion extremes provides an estimate of the impact of averaging the individual sweeps taken at 6.5-s intervals over 2 min (black dots); as anticipated, this calculation shows that the averaging approximates the ''no motion'' case, reinforcing the notion that averaging the typical wave motions to compute the mean tilt should produce acceptable results. The mean tilt on ships on which the FRSR is currently deployed is less than 2°, which suggests $\tau_{\lambda A}$ can be measured with an FRSR to an accuracy of 0.03 or better under most circumstances, assuming that the gain uncertainties are 2% and the absolute accuracy of $I_{\lambda 0}$ is known to 1.5%.

An interesting experiment is to calculate the uncertainty of a land-based FRSR whose orientation is perfectly known, and whose gain uncertainty is 2% and $I_{\lambda 0}$ uncertainty is 1.5%. This can be accomplished by omitting the orientation uncertainty term in (12). This calculation (black line in Fig. 6) shows that the land-based unit benefits from the ''lever arm'' property of the Langley technique, which allows $\tau_{\lambda A}$ to be estimated with increasing accuracy as the solar zenith angle increases. When an FRSR is mounted on a ship, the advantages of the lever arm are essentially offset by the increasing orientation uncertainty at high solar zenith angles; this produces a nearly constant uncertainty in $\tau_{\lambda A}(\sigma_{\tau_{\lambda A}})$ as a function of the solar zenith angle. Moreover, this offsetting effect suggests that the Langley technique itself cannot be performed under most conditions at sea. Thus, FRSRs deployed on ships must be calibrated on land.

Two additional experiments are to degrade the $I_{\lambda 0}$ uncertainty to 3.0% (dashed black line in Fig. 6), suggesting a poor knowledge of the extraterrestial spectrum, and the gain uncertainty to 4% (dashed blue line), suggesting significant drift over time. Either of these conditions can add 0.01–0.02 to $\sigma_{\tau_{\lambda A}}$. An increase in gain uncertainty is a much more likely scenario for an FRSR exposed to the elements during long deployments. It should be reinforced that the absolute uncertainty in $I_{\lambda 0}$ is a function of inaccurate specification of the reference spectrum and the ability to perform an accurate Langley calibration, while gain uncertainty is the result of degrading hardware components, such as interference filters and the diffuser material.

Companion experiments to calculate the uncertainty in the two-wavelength Ångström exponent, α, using (6) were performed (Fig. 7). Conditions were varied

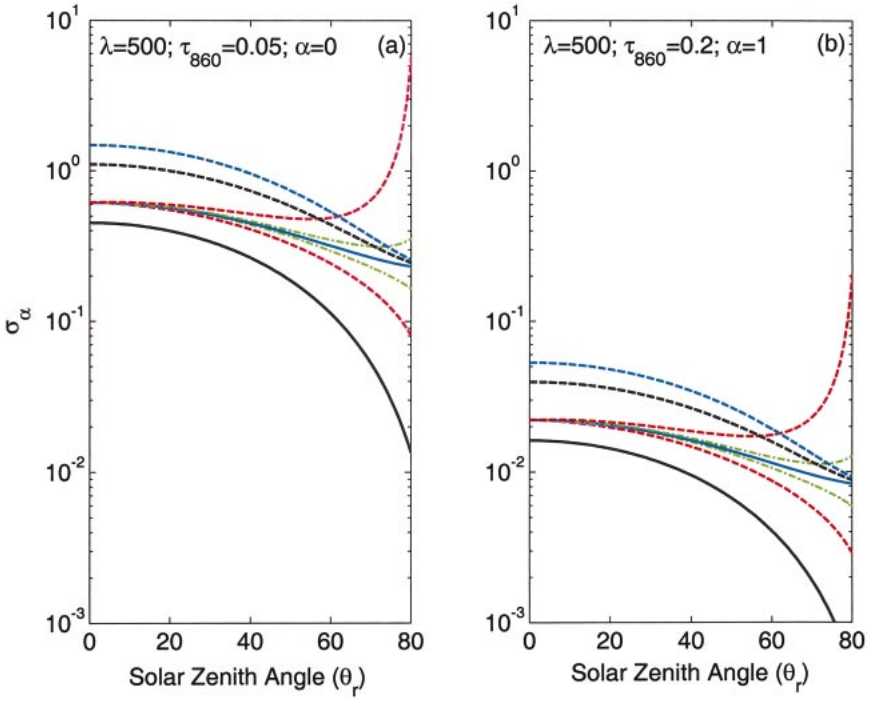

FIG. 7. As in Fig. 6 but for the Ångstrom exponent. (a) Plots of $\sigma_\alpha(\lambda_1, \lambda_2)$ vs θ_e for a clean maritime air mass ($\tau_{\lambda A} = 0.05$, $\alpha = 0$), where $\lambda_1 = 860$ nm and $\lambda_2 = 500$ nm, and (b) for a polluted air mass with ($\tau_{\lambda A} = 0.2$, $\alpha = 1$).

from clean ($\tau_{\lambda A} = 0.05$, $\alpha = 0$) to polluted ($\tau_{\lambda A} = 0.2$, $\alpha = 1$) air masses. The experiments demonstrate that the uncertainty in measuring α (σ_α) is a strong function of $\tau_{\lambda A}$ and α. As in previous experiments, the envelope of uncertainty for typical wave motion ($\pm 8°$) shows that (red dashed lines) σ_α is not particularly sensitive to the wave motion until the solar zenith angle exceeds 60°. The land versus ocean experiment once again reflects the fact that the lever-arm effect is offset by uncertainty in the position of the FRSR on a moving ship, producing a σ_α that is nearly independent of the solar zenith angle. Experiments with degradation in the uncertainty of knowledge of $I_{\lambda 0}$ (black dashed line) and with gain (blue dashed line) again show sensitivity to gain uncertainty.

The most striking aspect of the Ångström exponent uncertainty is that it is so much greater in clean air masses ($\tau_{\lambda A} = 0.05$, $\alpha = 0$), where it is approximately 0.6 in contrast to the polluted case, which is an order of magnitude lower. The plot also shows that this situation exists for land-based units. On the surface, this characteristic appears to be advantageous, since most applications of the FRSR involve polluted air; the downside is that it seems that the FRSR is unable to accurately measure the wavelength-dependent characteristics of marine aerosol (sea salt). While these aerosols contribute minimally to the local radiation budget, their spatial coverage over the world's oceans suggests that they could be important in the global radiation budget.

4. Conclusions

The analysis above presents an opportunity for data users to evaluate the uncertainty of each measurement made with the FRSR when it is deployed on a moving ship. Uncertainty in $\tau_{\lambda,A}$ and α can be computed (or estimated from this analysis) on the basis of the radiometer's orientation with respect to the sun, information about the quality of the radiometer gain calibration, and the integrity of determinations of $I_{\lambda 0}$. Once the uncertainties have been computed for each observation, they can be used as the filtering criteria for quality control or for hypothesis testing. In a typical experiment, it was found that the uncertainty in measurements of $\tau_{\lambda,A}$ is $\sim$0.03 at large zenith angles and $\sim$0.02 at small zenith angles. This uncertainty degrades to $\sim$0.04 at small solar zenith angles as the gain uncertainty doubles. Land-based FRSRs are likely to perform better, particularly at large solar zenith angles, due to the advantage of the ''lever-arm'' effect implicit in the Langley technique, perhaps reaching accuracies on the order of 0.02 or better. At sea, orientation uncertainty offsets the lever-arm effect, causing the uncertainty in measurements of $\tau_{\lambda,A}$ and α to be relatively sun-angle-independent, compared to land deployments. This offset also precludes

the use of the Langley technique at sea, so marine FRSRs must be calibrated on land. The Ångström exponent is difficult to measure in clean, maritime air masses, but this is more a function of the Langley technique itself than an artifact of the wave motion; similar difficulties would be encountered if the FRSR were mounted on a stabilized platform at sea or on land. It has been shown that the second derivative of α, which is α', is related to the aerosol size spectrum (O'Neill et al. 2001). For this application, it is clear that α' will have the same sensitivities as α, thereby making it difficult to retreive information about the aerosol size spectrum in clean, maritime air masses.

The FRSR uncertainties at sea are on the order of 0.02–0.03. This is slightly higher than uncertainties generally reported for land-based sun photometers, which are typically 0.01–0.02 (Schmidt et al. 1999). There are several reasons that the FRSR uncertainties are slightly larger than those for land-based units including orientation uncertainty, exposure to the elements, and inability to perform frequent Langley calibrations while at sea. Nonetheless, the FRSR uncertainties are acceptable for many applications and enable reasonably accurate, continuous estimates of $\tau_{\lambda,A}$ at sea.

One motivation for this work is the utility of marine shadow-band measurements of $\tau_{\lambda,A}$ and α to validate satellite estimates of same. To serve this function, an important question is: how accurate is the satellite retrieval likely to be and are the FRSR measurements more accurate? The accuracy and precision of satellite retrieval algorithms varies according to the configuration of the sensors and the methods used to estimate uncertainty are not uniform. Most uncertainty estimates are based on comparisons with surface-based sensors while others are based on model calculations. In general, the accuracy requirements for surface-based sensors are different depending on which satellite retrieval and application is under scrutiny.

A workshop was held in 1997 for the purpose of discussing passive remote sensing of tropospheric aerosols and an atmospheric correction for the aerosol effect (Kaufman et al. 1997). Based on this workshop, it was generally agreed that the accuracy of current multichannel satellite retrievals is estimated to be $\Delta\tau_{\lambda,A} =$ 0.03–0.05, where $\Delta\tau_{\lambda,A}$ is the accuracy of the retrieval. A later estimate of the accuracy of the Moderate Resolution Imaging Spectroradiometer (MODIS) retrieval suggested that $\Delta\tau_{\lambda,A} = 0.01 \pm 0.05\tau_{\lambda A}$ over the Atlantic Ocean off the southeast coast of the United States, based on comparisons with land-based sun photometers. This uncertainty estimate is better than the uncertainty projections made in the workshop in 1997, although the authors caution that more trials are needed in different aerosol regimes. The accuracy of satellite measurements of the Ångström exponent, α, is less certain, although comparisons with surface data suggest the systematic biases of 30% are possible (King et al. 1999). There is a caveat to these uncertainty estimates, however, since satellite aerosol retrievals are not attempted when $\tau_{\lambda A} \leq 0.1$. When $\tau_{\lambda A} \leq 0.1$, sea salt aerosol is assumed to be present and $\tau_{\lambda A}$ is specified as 0.1 and α is set to 0.

Based on the results of this workshop, one requirement for satellite validation measurements is that $\sigma_{\tau_{\lambda A}} \leq 0.03$ and $\sigma_{\alpha} \leq 0.3\alpha$ for many satellites. The results presented here suggest that a statistically significant number of FRSR measurements will have accuracy in the 0.02 range, since $\sigma_{\tau_{\lambda A}} \approx 0.03$ under many conditions, so the instrument should be useful as a source of satellite dataset validation in many instances. The instrument is designed to endure harsh conditions routinely encountered while operating continuously and autonomously on ships at sea. While it may be unable to achieve the accuracy of land-based units in many circumstances, it does provide a relatively accurate survey of aerosol optical conditions in open regions of the ocean, particularly if the region contains polluted air advected from continental areas. The simulations above suggest that the FRSR, if carefully calibrated, can meet these satellite validation requirements.

A second requirement is to understand the accuracy of the assumptions that are made when $\tau_{\lambda A} \leq 0.1$. Clearly, the most challenging situation for both satellites and FRSRs is measuring α in clean air masses. Fortuitously, this type of air mass is of lessor consequence for ocean color measurements and probably for climate forcing, though there are no definitive measurements and calculations to support the latter. It is likely that the α in these air masses is near zero, however, due to the mean size of sea salt particles, which is on the order of the size of small cloud droplets.

A main conclusion of this study is that the uncertainty in the exact position of the FRSR relative to the earth's coordinate system essentially offsets the lever-arm effect in the Langley technique. To a large extent, this is because the pitch and roll transducers used in the current FRSR design are accurate to only 0.5°. New technology that has recently become available promises to significantly reduce this uncertainty and eliminate the need for averaging. Hence, future versions of the FRSR promise to be considerably more accurate. Another important conclusion is that frequent calibrations are necessary to properly quantify gain and $I_{\lambda 0}$ uncertainty. Nonetheless, the current version of the marine FRSR appears to be a cost-effective means of collecting large amounts of satellite validation data over the world's oceans.

Acknowledgments. This work was supported under contract by the National Aeronautics and Space Administration (NASA) Sensor Intercomparison and Merger for Biological and Interdisciplinary Ocean Studies (SIMBIOS) program and the U.S. Department of Energy's Atmospheric Radiation Measurement program. The authors wish to acknowledge many people who, in addition to their own duties on various research vessels, have kindly offered their time to monitor our

instruments. The authors also wish to acknowledge Kirk Knoblespiesse and Dr. Christophe Pietras of the NASA Goddard Space Flight Center and Dr. Lee Harrison of the State University of New York for many useful discussions of various aspects of shadow-band radiometery. Finally, the authors acknowledge Scott Smith and Ray Edwards for invaluable technical assistance in the design of the marine FRSR.

APPENDIX

Estimates of $\sigma^2_{\tau_{\lambda R}}$ and $\sigma^2_{\tau_{\lambda O}}$

Uncertainty in the amount of molecular scattering ($\sigma^2_{\tau_{\lambda R}}$) and ozone absorption ($\sigma^2_{\tau_{\lambda O}}$) impact $\sigma^2_{\tau_{\lambda A}}$ and σ^2_{α}. Fluctuations in molecular scattering and ozone absorption are functions of atmospheric conditions, and the variance that they contribute depends on the accuracy with which the atmospheric conditions can be specified. Molecular scattering is well understood, so $\tau_{\lambda R}$ can be computed from theory using (Penndorf 1957)

$$\tau_{\lambda R} = \left(\frac{p}{p_0}\right)(a_1\lambda^4 + a_2\lambda^2 + a_3 + a_4\lambda^{-2})^{-1}. \quad \text{(A1)}$$

The variance equation for (8) is written as

$$\sigma^2_{\tau_{\lambda R}} = [p_0(a_1\lambda^4 + a_2\lambda^2 + a_3 + a_4\lambda^{-2})]^{-1}\sigma^2_p, \quad \text{(A2)}$$

where $(a_1, a_2, a_3, a_4) = (117.25, -1.32, 3.20 \times 10^{-4}, -7.68 \times 10^{-5})$, $p_0 = 1013.25$ hPa, and λ is given in microns. Uncertainty in the molecular scattering coefficients is assumed to be negligible. A conservative estimate of σ_p is 60 hPa, which represents the full range of observed atmospheric pressures (980–1040 hPa) and therefore serves as an upper bound. With $\sigma_p = 60$ hPa, $\sigma_{\tau_{\lambda R}}$ ranges from a maximum of 1.7×10^{-10} at 415 nm to a minimum of 9.1×10^{-12} at 862 nm, which shows that molecular scattering does not contribute significantly to $\sigma^2_{\tau_{\lambda A}}$. To summarize, despite a reasonable error in the specification of p, the impact on $\sigma^2_{\tau_{\lambda A}}$ is negligible and is heretofore neglected. It is noted that failure to subtract $\tau_{\lambda R}$ when computing the actual value of $\tau_{\lambda A}$ (as opposed to the uncertainty) will lead to a large error in the 400–500-nm wavelength bands.

Ozone absorption is also well understood, so $\sigma^2_{\tau_{\lambda O}}$ can be computed from theory if the amount of ozone in the atmospheric column is known. The total ozone in a column, ξ, is typically measured in units of 10^{-3} cm of gas reduced to standard temperature and pressure [Dobson Unit (DU)]. Ozone absorption is computed by multiplying the total column ozone by an absorption coefficient, k_λ, determined from laboratory measurements. The impact of ozone absorption on the optical thickness is expressed as

$$\tau_{\lambda O} = \xi k_\lambda, \quad \text{(A3)}$$

and the corresponding variance from the ozone contribution to $\sigma^2_{\tau_{\lambda A}}$ is

TABLE A1. Ozone absorption coefficients for FRSR center wavelengths.

λ (nm)	(1000 DU^{-1})
415	0.0084
500	0.0328
615	0.1140
670	0.0449
870	0.0036

$$\sigma^2_{\tau_{\lambda O}} = k^2_\lambda\sigma^2_\xi + \xi^2\sigma^2_{k_\lambda}. \quad \text{(A4)}$$

Assuming that k_λ is known to great accuracy, $\sigma^2_{k_\lambda} \simeq 0$. The upper bound of the ozone contribution to $\sigma^2_{\tau_{\lambda A}}$ can be computed by assuming that $\sigma_\xi = 200$ DU, which is the planetary range typically observed by the Total Ozone Mapping Spectrometer satellite. The ozone absorption coefficients for the wavelength bands of the shadow-band radiometer are given in Table A1 (M. Wang 2000, personal communication). Calculations show that $\sigma_{\tau_{\lambda O}} \approx 0.02$ at $\lambda = 610$ nm and $\sigma_{\tau_{\lambda O}} \approx 0.01$ at $\lambda = 660$ nm, and $\sigma_{\tau_{\lambda O}} < 0.01$ otherwise. Assuming that σ_ξ is far less than 200 DU, these calculations show that $\sigma^2_{\tau_{\lambda O}}$ may not contribute significantly to $\sigma^2_{\tau_{\lambda A}}$, even in the vicinity of 600–700 nm. Failure to include the impact of $\tau_{\lambda O}$ when computing $\tau_{\lambda A}$ will have a detrimental impact on the accuracy of $\tau_{\lambda A}$, particularly in the vicinity of 600–700 nm.

REFERENCES

Ångström, A., 1961: Techniques for determining the turbidity of the atmosphere. *Tellus,* **13,** 214–223.

Berk, A., L. S. Bernstein, and D. C. Robertson, 1990: MODTRAN: A moderate resolution model for LOWTRAN7. Geophysical Directorate Phillips Laboratory Tech. Rep. GL-TR-90-0122, Hanscom AFB, MA, 44 pp.

Colina, R., C. Bohlin, and F. Castelli, 1996: The 0.12–2.5 micrometer absolute flux distribution of the sun for comparison with solar analog stars. *Astron. J.,* **112,** 307–315.

Gordon, H. R., and M. Wang, 1994: Retrieval of water-leaving radiance and aerosol optical thickness over oceans with SeaWiFS: A preliminary algorithm. *Appl. Opt.,* **33,** 443–152.

Guzzi, R., G. Maracci, R. Rizzi, and A. Siccardi, 1985: Spectroradiometer for ground-based atmospheric measurements related to remote sensing in the visible from a satellite. *Appl. Opt.,* **24,** 2859–2864.

Harrison, L., and J. Michalsky, 1994: Objective algorithms for retrieval of optical depths from ground-based measurements. *Appl. Opt.,* **33,** 5126–5132.

——, ——, and J. Berndt, 1994: Automated multifilter rotating shadow-band radiometer: An instrument for optical depth and radiation measurements. *Appl. Opt.,* **33,** 5118–5125.

Kaufman, Y. J., and Coauthors, 1997: Passive remote sensing of tropospheric aerosol and atmospheric correction for the aerosol effect. *J. Geophys. Res.,* **102,** 16 815–16 830.

King, M. D., Y. J. Kaufman, D. Tanré and T. Nakajima, 1999: Remote sensing of tropospheric aerosols from space: Past, present, and future. *Bull. Amer. Meteor. Soc.,* **80,** 2229–2259.

Meyer, S. L., 1992: *Data Analysis for Scientists and Engineers.* Peer Management Consultants, 511 pp.

Neckel, H., and D. Labs, 1984: The solar radiation between 3300 and 12500 Å. *Sol. Phys.,* **90,** 205–258.

O'Neill, N. T., T. F. Eck, B. N. Holben, A. Smirnov, and O. Dubovik,

2001: Bimodal size distribution influences on the variation of Ångström derivatives in spectral and optical depth space. *J. Geophys. Res.,* **106** (D9), 9787–9806.

Penndorf, R., 1957: Tables of the refractive index for standard air and the Rayleigh scattering coefficient for the spectral region between 0.2 and 20.0 micron and their application. *J. Opt. Soc. Amer.,* **47,** 176–182.

Porter, J. N., M. A. Miller, C. Motell, and C. Pietras, 2001: Use of handheld sun photometers for measurements of aerosol optical thickness at sea. *J. Atmos. Oceanic Technol.,* **18,** 765–774.

Reynolds, M. R., M. A. Miller, and M. J. Bartholomew, 2001: A fast-rotating, spectral shadow-band radiometer for marine applications. *J. Atmos. Oceanic Technol.,* **18,** 200–214.

Russell, P. B., J. M. Livingston, and E. E. Uthe, 1979: Aerosol-induced albedo change: Measuring and modeling of an incident. *J. Atmos. Sci.,* **36,** 1587–1608.

——, and Coauthors, 1993: Pinatubo and pre-Pinatubo optical depth spectra: Mauna Loa measurements, comparisons, inferred particle size distributions, radiative effects, and relationship to lidar data. *J. Geophys. Res.,* **98,** 22 969–22 985.

Schmidt, B., and C. Wehrli, 1995: Comparison of sun photometer calibration by use of the Langley technique and the standard lamp. *Appl. Opt.,* **34,** 4500–4512.

——, and Coauthors, 1999: Comparison of aerosol optical depth from four solar radiometers during the fall 1997 ARM intensive observation period. *Geophys. Res. Lett.,* **26,** 2725–2728.

Shaw, G. E., 1983: Sun photometry. *Bull. Amer. Meteor. Soc.,* **64,** 4–10.

Thuiller, G., M. Herse, P. C. Simon, D. Labs, H. Mandel, and D. Gillotay, 1998: Observations of the solar spectral irradiance from 200 nm to 870 nm during the ATLAS 1 and ATLAS 2 missions by the SOLSPEC spectrometer. *Metrologia,* **35,** 689–695.

——, ——, ——, ——, ——, ——, and T. Foujols, 2003: The solar spectral irradiance from 200 to 2400 nm as measured by the SOLSPEC spectrometer from the ATLAS 1-2-3 and EURECA missions. *Sol. Phys.,* **214,** 1–22.

Wehrli, C., 1985: Extraterrestrial solar spectrum. Physikalisch-Meteorologisches Observatorium and World Radiation Center Publ. 615, Davos Dorf, Switzerland. [Available online at http://rredc.nrel.gov/solar/standards/am0/.]